A comprehensive dynamic modeling approach for giant magnetostrictive material actuators

2013 Smart Mater. Struct. 22 125005

(http://iopscience.iop.org/0964-1726/22/12/125005)

Smart Mater. Struct. 22 (2013) 125005 (10pp) doi:10.1088/0964-1726/22/12/125005

A comprehensive dynamic modeling approach for giant magnetostrictive material actuators

Guo-Ying Gu[1], Zhi Li[2], Li-Min Zhu[1] and Chun-Yi Su[2,3]

[1] State Key Laboratory of Mechanical System and Vibration, School of Mechanical Engineering, Shanghai Jiao Tong University, 200240, People's Republic of China
[2] Department of Mechanical and Industrial Engineering, Concordia University, Montreal, QC H3G1M8, Canada
[3] College of Automation Science and Engineering, South China University of Technology, Guangzhou 510641, People's Republic of China

E-mail: guguoying@sjtu.edu.cn

Received 4 June 2013, in final form 8 October 2013
Published 1 November 2013
Online at stacks.iop.org/SMS/22/125005

Abstract
In this paper, a comprehensive modeling approach for a giant magnetostrictive material actuator (GMMA) is proposed based on the description of nonlinear electromagnetic behavior, the magnetostrictive effect and frequency response of the mechanical dynamics. It maps the relationships between current and magnetic flux at the electromagnetic part to force and displacement at the mechanical part in a lumped parameter form. Towards this modeling approach, the nonlinear hysteresis effect of the GMMA appearing only in the electrical part is separated from the linear dynamic plant in the mechanical part. Thus, a two-module dynamic model is developed to completely characterize the hysteresis nonlinearity and the dynamic behaviors of the GMMA. The first module is a static hysteresis model to describe the hysteresis nonlinearity, and the cascaded second module is a linear dynamic plant to represent the dynamic behavior. To validate the proposed dynamic model, an experimental platform is established. Then, the linear dynamic part and the nonlinear hysteresis part of the proposed model are identified in sequence. For the linear part, an approach based on axiomatic design theory is adopted. For the nonlinear part, a Prandtl–Ishlinskii model is introduced to describe the hysteresis nonlinearity and a constrained quadratic optimization method is utilized to identify its coefficients. Finally, experimental tests are conducted to demonstrate the effectiveness of the proposed dynamic model and the corresponding identification method.

(Some figures may appear in colour only in the online journal)

1. Introduction

Smart material actuated nanopositioning stages are becoming popular in a wide range of precision equipment with nanometer or sub-nanometer displacement resolution [1]. In this equipment, piezoelectric ceramic actuators are widely applied to realize the actuation due to their advantages of large output force, fast response time and easy electrical control [2]. However, there is an increasing demand for more force and larger strain with other smart material based actuators [3–5]. Among the possible options, a giant magnetostrictive material actuator (GMMA) is the best choice. In technical terms, Terfenol-D is the most famous commercially available giant magnetostrictive material (GMM), which is a rare earth–iron alloy of terbium, dysprosium, and iron metals. In comparison to other GMMs, the Terfenol-D based GMMA offers the largest room-temperature magnetostriction [6, 7].

The GMMA works on the principle of magnetostriction, which is a physical coupling phenomenon between magnetic properties and mechanical properties [6, 7]. In other words, strains are generated by an applied magnetic field, which is known as the Joule effect; conversely, mechanical stresses

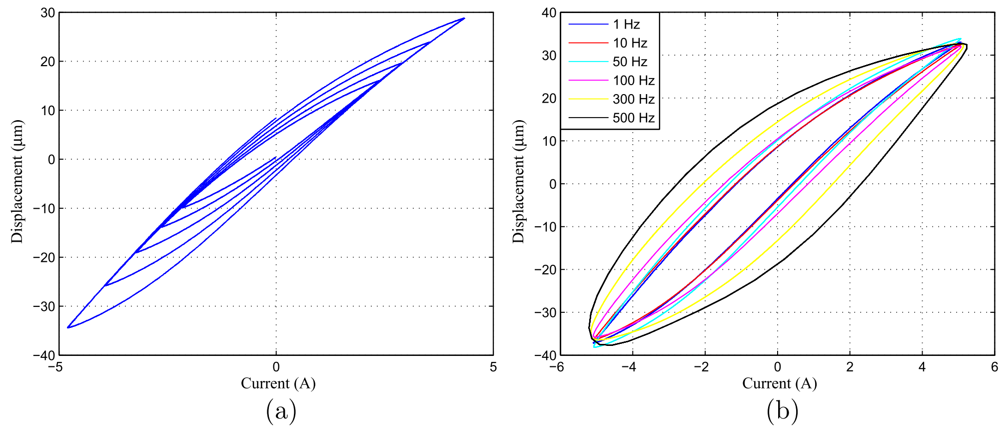

Figure 1. Hysteresis loops of a GMMA containing the bias permanent magnetic. (a) Different input amplitudes. (b) Different input frequencies.

imposed on the GMM can produce measurable changes in magnetization, known as the Villari effect [8]. According to these two famous effects, both actuation and sensing functions can be achieved by the GMM. In this paper, we focus on the Joule effect for the purpose of actuation.

Similar to other smart materials based actuators (i.e. piezoelectric ceramic actuators and shape memory alloy actuators), GMMAs exhibit a strong intrinsic non-smooth hysteresis nonlinearity with both amplitude-dependent and frequency-dependent behaviors, as shown in figure 1. Hysteresis usually degrades the system performance in such a manner as to give rise to undesirable inaccuracy or oscillations, even leading to instability [9]. In order to remedy the hysteresis, the first step is to develop an available model for the accurate description of the hysteresis. On the basis of the principles of physics, the Jiles–Atherton model [10] was developed to describe the hysteresis behavior using the domain wall theory and extensive works have since been developed in [11–13]. Alternatively, without considering the physical insight into the problem, the Preisach model [14–18] was used to describe the hysteresis nonlinearity using the elementary hysteresis operator with a simple mathematical structure. Although the Preisach model is efficient for hysteresis modeling of GMMAs, it is quite a challenge to construct its analytical inverse and to develop a real-time controller because of the great computational costs for calculation and identification. As a subclass of the Preisach model, the Prandtl–Ishlinskii (PI) model is defined in terms of the superposition of elementary play operators or stop operators with a density function. The PI model is effective in describing the hysteresis nonlinearity by a single threshold variable [19]. The main advantages of the PI model over the Preisach model are the reduced modeling complexity and the analytical inverse for the PI model, thus making it more efficient for real-time applications [20, 21]. The reader may refer to [3] for a recent review of the hysteresis models for GMMAs.

Through the above literature review, many efforts have been made towards modeling the GMMAs. However, the previous attention was mainly focused on the static input–output hysteresis nonlinearity without considering the dynamic behaviors of GMMAs. Even if a phenomenological Preisach model and a linear dynamic model were combined in [15, 16] to describe the dynamic behaviors of the GMMAs, the physical insight of the magnetostrictive actuators was not taken into account. Recently, based on the Jiles–Atherton model, some coupled magneto-elastic models have been presented [22–24], in which the magnetic and magnetostrictive hysteresis was modeled with no current. In addition, the analysis was limited to magnetostrictive rods, without considering the entire actuator structure. However, GMMAs typically employ current-carrying winding coils to produce a magnetic field. It is inadequate for current-carrying applications. Based on the linear magneto-mechanical equations, Braghin *et al* [25] recently developed a linear dynamic model of the GMMA for active vibration control. However, the nonlinear hysteresis behavior of the GMMA was not considered. Up to now, few works have dealt with complete dynamic behavioral descriptions of GMMAs.

For such motivations, this paper presents a novel comprehensive modeling approach to completely describe the dynamic behaviors of GMMAs based on descriptions of nonlinear electromagnetic behavior, the magnetostrictive effect and the frequency response of the mechanical dynamics. Towards this modeling approach, a two-module comprehensive model with a two-order linear dynamic plant preceded by an input hysteresis nonlinearity is developed. In order to validate the developed model, the linear dynamic part and the nonlinear hysteresis part of the proposed comprehensive model are identified in sequence. For the linear part, an approach based on axiomatic design theory is adopted. For the nonlinear part, a Prandtl–Ishlinskii model is introduced to describe the hysteresis nonlinearity and a constrained quadratic optimization method is utilized to identify the coefficients of the hysteresis model. Finally, a prototype platform is built and experimental tests are conducted. The experimental and simulation results clearly verify the effectiveness of the proposed comprehensive model and the corresponding identification method.

The remainder of this paper is organized as follows. Section 2 states the comprehensive modeling approach,

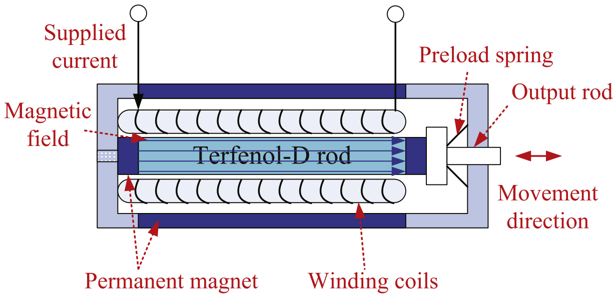

Figure 2. Schematic illustration of a Terfenol-D based magnetostrictive actuator.

section 3 details the model validation with experimental results of the GMMA and section 4 concludes this paper.

2. Comprehensive modeling approach

2.1. Description of a GMMA

A GMMA is schematically shown in figure 2. It consists mainly of current-carrying winding coils, a movable Terfenol-D drive rod surrounded by the winding coils, a bias permanent magnetic that produces the bidirectional movement of the rod, a pair of preloaded springs and an output rod attached to the Terfenol-D rod. The drive rod produces a stroke and output force by the moving magnetic field generated by the current-carrying winding coils on the physical principles of Terfenol-D. The preloaded springs and the bias permanent magnets are utilized to produce bidirectional movement of the Terfenol-D rod. Since the Terfenol-D rod can produce a large stroke and output force, no additional mechanism is designed to amplify the output motion. Before the following model development, two common assumptions are introduced [6, 26, 27]: (i) no flux leakage losses and ideal flux linkage; (ii) uniform magnetic flux density distribution throughout the Terfenol-D rod.

2.2. Comprehensive model of the GMMA

As shown in figure 2, when the supplied current i is applied through the winding coils, the magnetic field H_N is created in the area along the Terfenol-D rod. According to Ampere's law, the magnetic field applied to the Terfenol-D rod is related to the current i by the relation $H_N = Ni/l$, where l is the length of the Terfenol-D rod and N is the number of coil turns. The magnetic flux density B_N is then obtained by the constitutive equation $B_N = \mu_0\mu_r H_N$, where μ_0 and μ_r are the free permeability and relative permeability respectively. The magnetic flux Φ_N related to the magnetic flux density B_N is obtained as $\Phi_N = \int_A B_N \, dA$, where A is the cross-sectional surface area. With a uniform magnetic flux density distribution, the flux Φ_N is derived as $\Phi_N = B_N A_r$, where A_r is the cross-sectional area of the Terfenol-D rod. In the presence of the magnetic flux, small magnetic domains [26, 28] rotate or re-orient themselves to cause internal strain in the Terfenol-D structure due to the magnetostrictive effect. As a result, the Terfenol-D rod stretches along the direction of the magnetic field to exert a force F_A on the output rod of the actuator, thus producing a displacement x. In addition to the generated magnetic flux Φ_N, mechanical stresses imposed on the GMMA in turn produce an induced magnetic flux Φ_T in the Terfenol-D rod [22, 28, 29]. Therefore, the total flux Φ in the Terfenol-D rod consists of two parts, expressed as

$$\Phi = \Phi_N + \Phi_T. \tag{1}$$

Remark. It should be noted that the GMMA works on the principle of magnetostriction, which is a physical coupling phenomenon between magnetic properties and mechanical properties. Therefore, strains are generated in response to an applied magnetic field; conversely, mechanical stresses imposed on the GMMA can produce measurable changes in magnetization. These two effects are reflected in the first and second terms in (1).

To further characterize the coupling electro-magneto-mechanical behavior of the magnetostrictive actuator, it is essential to describe the coupling relationship of the supplied current i in the electric domain and the generated force F_A in the mechanical domain, i.e. a representation of i versus F_A. Previous studies [3, 15, 28] have shown that ferromagnetic materials present a nonlinear relationship between the magnetic flux Φ and field H_N (well known as hysteresis). The hysteresis is an inherent nonlinear effect because of loss phenomena [30, 31] taking place inside magnetostrictive materials. Since the variable magnetic field H_N in magnetostrictive actuators is produced by employing a current i through the winding coils, hysteresis can be taken into account by adding a so-called current loss term i_H corresponding to the dissipated hysteresis loss [30] in the expression for the supplied current i. Considering its non-smooth and non-memoryless nature as well as multi-valuedness, hysteresis makes the modeling and control task quite challenging [32]. In this paper, a nonlinear operator P is introduced to represent the dissipation of hysteresis loss, which can be described by the hysteresis models [3, 11, 19, 33], for example, Jiles–Atherton, Preisach and Prandtl–Ishlinskii models, through experimental data. In this way, the current loss term i_H due to the hysteresis is denoted as $i_H = P(\Phi)$. The supplied current i for the GMMA is thereby governed by

$$i = i_T + P(\Phi) \tag{2}$$

where $i_T = i - i_H$ is regarded as the current to generate mechanical force in the anhysteretic case.

Thus far, the hysteresis nonlinearity is separated in the electrical domain as described in (2). In the anhysteretic case, the linear two-part constitutive representation [34, 35] based upon reducing the expansion of the Gibbs free energy equation is used to characterize the coupling electro-magneto-mechanical behavior by relating the electrical current i_T and magnetic flux Φ to the force F_A and position x. Under clamped conditions, i.e. $x = 0$, the generated magnetic

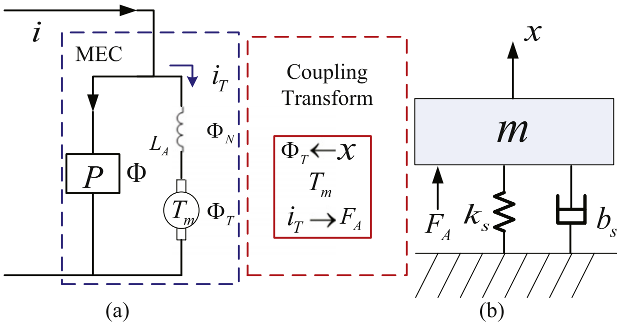

Figure 3. Schematic representation of the proposed comprehensive dynamic model of the magnetostrictive actuator. (a) Electrical submodel. (b) Mechanical submodel.

flux through the Terfenol-D rod is defined by the clamped inductance L_A of the coils as follows [34, 35]

$$\Phi = \Phi_N = L_A i_T. \tag{3}$$

At the same time, the generated force can be obtained by

$$F_A = T_{em} i_T \tag{4}$$

where T_{em} is the electromechanical transduction coefficient. In addition, according to (1), by setting the applied electrical current to be zero, the magnetic flux induced from the mechanical part as an external stress applied to the actuator output rod is expressed as [6, 7, 34, 35]

$$\Phi = \Phi_T = T_{me} x \tag{5}$$

where T_{me} is the mechanoelectric transduction coefficient. Note that the transduction coefficients T_{em} and T_{me} represent the ability of transducers to convert electrical energy to mechanical energy or vice versa, generally satisfying $T_{em} = T_{me} = T_m$ [34, 35].

With respect to the generated force F_A, the mechanical dynamic behavior of the actuator [27, 36] can be modeled as a mass–spring–damper system in a frequency band within the first mechanical mode of vibration according to Newton's laws of motion

$$m\ddot{x}(t) + b_s\dot{x}(t) + k_s x(t) = F_A \tag{6}$$

where m is the equivalent mass of the moving part, b_s is the equivalent damping coefficient, and k_s is the equivalent stiffness.

Through the above discussions and notations, the complete electro-magneto-mechanical model, including nonlinear electro-magnetic behavior, the magnetostrictive effect and the frequency response of the mechanical part is developed, which can be schematically represented in figure 3. It maps the relationships between current and magnetic flux at the electromagnetic part to the force and displacement at the mechanical part in a lumped parameter form. As shown in figure 3(a), an electrical submodel, consisting of a nonlinear hysteresis operator P, a linear inductance L_A and a magnetostrictive transformer T_m, is constructed to describe the nonlinear electrical behavior, where P accounts for the hysteresis effect and i_H is the current loss due to this effect; T_m electrically in series with the inductance L_A represents

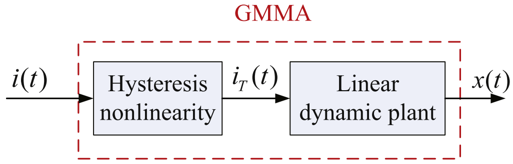

Figure 4. Block diagram of the comprehensive model.

the magnetostrictive effect, which is an electromechanical transducer with a transformer ratio. In the mechanical part, the lumped mass–spring–damper mechanical system is represented in figure 3(b).

Substituting (2), (4) and (5) into (6), the comprehensive dynamic model is expressed as

$$\ddot{x}(t) + 2\xi\omega_n\dot{x}(t) + \omega_n^2 x(t) = K\omega_n^2 i_T(t) \tag{7}$$

$$i_T(t) = P'(i(t)) \tag{8}$$

with $2\xi\omega_n = b_s/m$, $\omega_n^2 = k_s/m$ and $K\omega_n^2 = T_m/m$, where a new hysteresis operator $P'(i(t))$ is introduced for convenience of the following identification and verification. It should be noted that $i_T(t)$ is an internal variable which cannot be directly measured.

From (7) to (8), the two-module comprehensive model is developed to completely describe the behaviors of the GMMA. The first module is a nonlinear hysteresis model to describe the hysteresis nonlinearity, and the cascaded second module is a linear second-order dynamic plant to represent the dynamic behavior. For illustration, the block diagram of the comprehensive model is schematically shown in figure 4.

Remark. (i) The comprehensive modeling approach for the GMMA is proposed based on descriptions of nonlinear electro-magnetic behavior, the magnetostrictive effect and the frequency response of the mechanical dynamics. Towards this modeling approach, a nonlinear operator is introduced to represent the dissipation of hysteresis loss in the electrical domain. In this case, the nonlinear hysteresis effect is characterized in the electrical part, and is separated from the linear dynamic plant in the mechanical part. Finally, a two-module dynamic model is developed to account for both the dynamics of the GMMA and the hysteresis inherent to the GMM. As far as the authors know, there is no such complete description in the literature, although many efforts have been made, such as [3, 15, 16, 20, 22–25, 37, 38]. Most of the available results have focused on a static input–output hysteresis nonlinearity, i.e., [3, 20, 37, 38], where the dynamic behaviors of GMMAs were not considered. Although a phenomenological Preisach model and a linear dynamic model [15, 16] were combined to describe the dynamic behaviors of the GMMAs, they had no strong physical base. On the other hand, the current was not taken into account in the models [22–24], which was inadequate for current-carrying applications. In the following development, the proposed model will be justified by the experimental results.

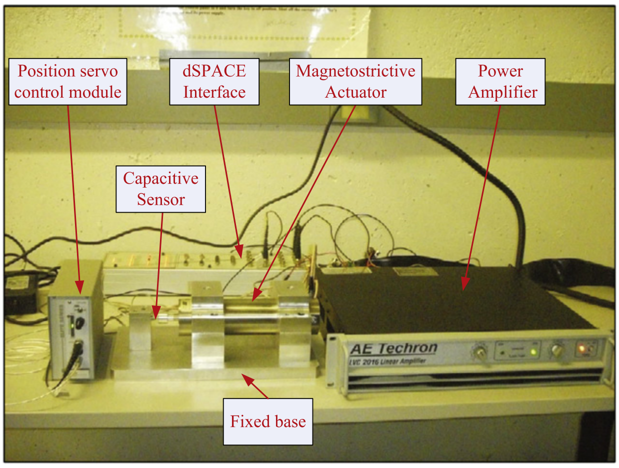

Figure 5. Architecture of the experimental platform.

(ii) It should be noted that with the proposed dynamic modeling approach, the GMMA is described as a linear second-order dynamic plant preceded by the input hysteresis nonlinearity. This structure is similar to those of the piezoelectric actuators [2, 36]. Therefore, the available control approaches for piezoelectric actuators can be introduced to control the GMMA with the developed dynamic model.

3. Model validation

3.1. Experimental platform

In order to validate the proposed model of GMMAs, an experimental platform is established, as shown in figure 5. It consists of the following five parts: a GMMA with a fixed base, a displacement sensor module, a power amplifier, a DSPACE-DS1104 control board and a personal computer for real-time rapid prototyping development. The GMMA is an ETREMA standard actuator (Model 100LLSSE) with 100 μm displacement. The power amplifier (Model LVC2016 produced by AE Techron Inc.) operates on a current control mode to generate the supplied current for the GMMA. A capacitive position sensor (CPS, Model C23-C) is utilized to measure the actual displacement of the actuator and a position servo-control module (PSCM, Model CPL190) is adopted to transfer the displacement to analog voltage in the range -10 to 10 V. The displacement sensor module is produced by Lion Precision Inc. and the sensitivity of the CPS is 80 mV μm^{-1}. A dSPACE control board equipped with 16-bit analog to digital converters (ADCs) and 16-bit digital to analog converters (DACs) is used to realize real-time hardware-in-the-loop control using the MATLAB/Simulink environment. As an illustration, figure 6 shows a block diagram of the above experimental platform.

3.2. Model identification

Towards the developed comprehensive model of the GMMA, the linear dynamic submodel (7) and the nonlinear hysteresis submodel (8) are cascaded. Due to the existence of the hysteresis nonlinearity, there has been no general approach to identify the parameters for the comprehensive model until now. As a compromise, the commonly adopted approach in the literature is to identify the linear submodel and nonlinear submodel separately by leveraging their special characteristics [2, 39]. In the following development we will follow this line.

3.2.1. Identification of the linear dynamic subsystem. Inspired by the recent work in [40], the axiomatic design theory (ADT) based approach is utilized in this work to identify the parameters of the linear dynamic subsystem (7). With the idea of the ADT-based approach, the overall functional requirements (FRs) corresponding to the system dynamic responses are broken down into near-decoupled sub-functional requirements. Therefore, the identified parameters (IPs) of the system model is determined to satisfy the sub-functional requirements [40] using the experimental data. The step response of the system can be used to determine the parameters K, ξ and ω_n in (7), where K is the ratio of the displacement to the applied current in the steady state, and ξ and ω_n can be determined by using the following set of equations (9) or (10)

$$\xi = \frac{4t_p}{\sqrt{(\pi t_s)^2 + (4t_p)^2}} \qquad \omega_n = \frac{\sqrt{(\pi t_s)^2 + (4t_p)^2}}{t_s t_p} \tag{9}$$

$$\xi = \frac{-\ln(\mathrm{os})}{\sqrt{\pi^2 + (\ln(\mathrm{os}))^2}} \qquad \omega_n = \frac{\pi}{t_p\sqrt{1-\xi^2}}. \tag{10}$$

where t_p is the peak time, t_s is the settling time, and os is the percentage overshoot. In addition, sinusoids with broadband frequencies or band-limited white noise signals can be typically used as excitation signals to the plant system, and a magnitude plot is formed to directly obtain the resonant frequency ω_n.

A near-decoupled ADT-based identified hierarchy is constructed in this work, as shown in figure 7. Experiments are then conducted to identify the system parameters. It is well known that the GMMA has severe nonlinearities such as hysteresis over large displacements, and creep over long time periods [20]. In order to estimate the parameters of the linear part of the proposed model as accurately as possible, small-amplitude input current should be supplied to avoid distortion from hysteresis, as generally reported in the literature [2, 41]. Also, a higher sampling frequency of 20 kHz is set to capture the fast dynamic response of the system in the first 6 ms when the creep behavior can be conservatively neglected. The following algorithm is used in this work to determine these FRs and IPs illustrated in figure 7.

Step 1. Low-amplitude ($|i(t)| < 0.6$ A) band-limited white noise excitation signals are applied to the part. With

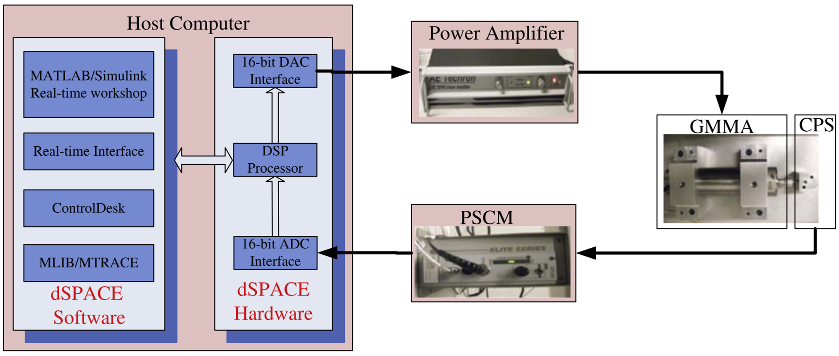

Figure 6. Block diagram of the experimental platform.

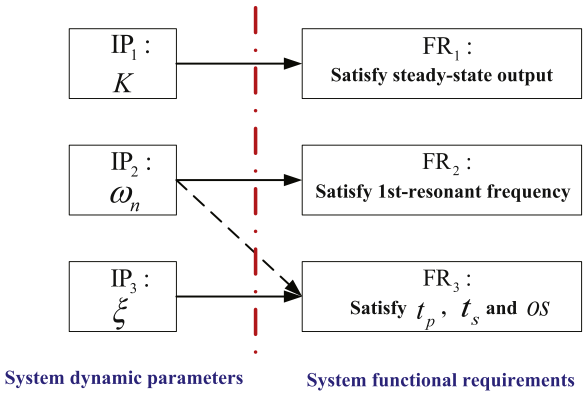

Figure 7. Identified hierarchy of a near-decoupled ADT-based approach.

the sampled input current and output displacement of the system, a Bode plot is formed by using System Identification Tool (*ident*) in MATLAB. Then, ω_n is obtained from the first resonant frequency in the magnitude plot.

Step 2. The low-amplitude step response ($i(t) = 0.726$ A) of the plant is captured. With the analysis of the transient response, the steady-state output, the times t_p and t_s and the percentage overshoot os can be derived.

Step 3. With the steady-state output of the stable step response, the parameter K can be obtained.

Step 4. By using (10), the parameter ξ is derived with the step response characteristics obtained in *Step* 2.

Based on the proposed approach and algorithm, the system parameters in (7) are determined as $K = 4.4$, $\xi = 0.28$ and $\omega_n = 2\pi \times 3200$ (rad s^{-1}). Therefore, the transfer function of the linear dynamic plant (7) can be obtained as follows:

$$G(s) = \frac{1.7787 \times 10^9}{s^2 + 11\,259s + 4.0426 \times 10^8}. \tag{11}$$

To verify the identified parameters, figure 8 shows the comparison of experimental data and model simulation data. It can be clearly observed that the developed dynamic model with the identified parameters closely follows the dynamic response of the tested GMMA.

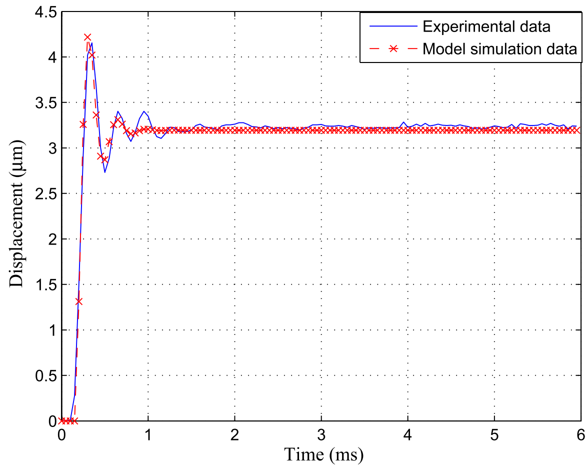

Figure 8. Comparison of the experimental response and model simulation response: blue solid—experimental data; red dash star—model simulation data.

3.2.2. Description of the hysteresis nonlinearity. With the identified parameters of the linear dynamic part (11), the following step is to describe and identify the hysteresis nonlinearity (8). There are many available hysteresis models to describe the hysteresis of GMMAs. The reader may refer to [3] for a recent review. In this work, just for the purpose of model validation, a modified Prandtl–Ishlinskii (MPI) model [33] is selected as an illustration. Certainly, other hysteresis models, such as the Jiles–Atherton model and the Preisach model, can also be selected depending on the different applications.

With the MPI model, the hysteresis nonlinearity in (8) can be described as follows:

$$i_\mathrm{T}(t) = g(i(t)) + \sum_{i=1}^{n} b(r_i) F_\mathrm{r}[i](t)\,\mathrm{d}r \tag{12}$$

where $g(i(t)) = a_1 i^3(t) + a_2 i^2(t) + a_3 i(t) + a_4$ is selected in this work to adjust the overall shape of the hysteresis loop; $b(r_i)$ is the weighted coefficient at the threshold of r_i; n is the number of the play operators used for identification; $F_r[i](t)$ is the classical play operator defined as

$$\begin{aligned} F_\mathrm{r}[i](0) &= f_\mathrm{r}(i(0), 0) \\ F_\mathrm{r}[i](t) &= f_\mathrm{r}(i(t), F_\mathrm{r}[i](t_i)) \end{aligned} \tag{13}$$

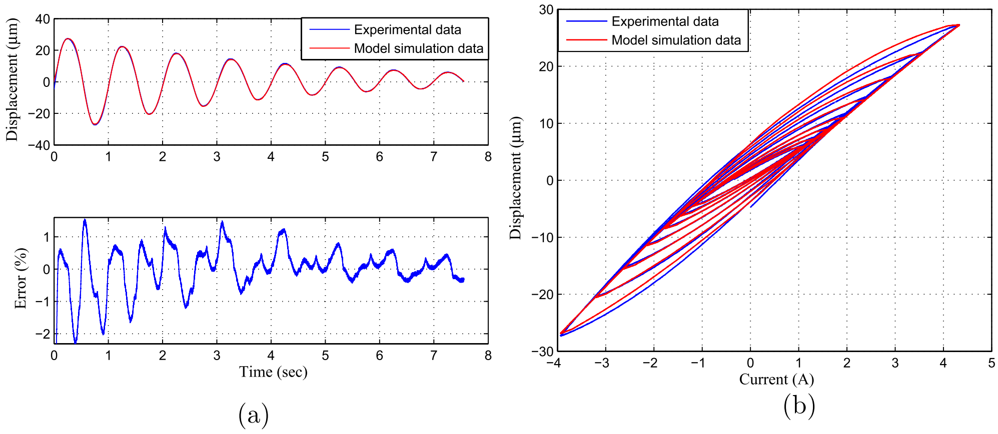

Figure 9. Comparisons of experimental data and comprehensive model output. (a) Displacement versus time. (b) Hysteresis loop.

for $t_i < t \leq t_{i+1}, 0 \leq i \leq N-1$ with

$$f_r(v, w) = \max(v - r, \min(v + r, w)) \tag{14}$$

where $0 = t_0 < t_1 < \cdots < t_N = t_E$ is a partition of $[0, t_E]$, such that the input current $i(t)$ is monotone on each of the subintervals $[t_i, t_{i+1}]$. It should be noted that the selection of $g(i)$ in the MPI model (12) has no general criterion, which provides a certain freedom for the designers to extend it [33]. In this work, a third-order polynomial function is selected on the basis of the prior experimental data.

To identify the coefficients of the hysteresis model (12), a specific amplitude-decreasing sinusoidal signal is designed to drive the GMMA. The frequency of the input is chosen as 1 Hz to avoid exciting the dynamic response of the system. After the parameters of the linear dynamic subsystem have been determined, the hysteresis output can be approximately calculated by the inverse of the linear dynamic subsystem (11). Thus, the weighted coefficient $b(r_i)$ and the coefficients of the third-order polynomial function a_i in (12) can be obtained by the following constrained quadratic optimization

$$\min\{[\mathbf{Cp} - d]^{\mathrm{T}}[\mathbf{Cp} - d]\} \tag{15}$$

with constraints

$$p(i) \geq 0, \qquad i \in \{1, 2, 3, \ldots, 20\} \tag{16}$$

where $\mathbf{p} = [b(r_1), \ldots, b(r_{16}), -a_1, -a_2, a_3, a_4]^{\mathrm{T}}$, $\mathbf{C} = [F_{r_1}, \ldots, F_{r_{16}}, i^3, i^2, i, 1]$, d is the calculated hysteresis output. Based on the nonlinear least-square optimization toolbox in MATLAB, the parameters of the MPI model are identified using the experimental data which are listed in table 1.

With the identified model parameters, figure 9 shows the comparisons of the experimental results and simulation results of the identified comprehensive model. Figure 9(a) shows the model prediction performance with the modeling error, and figure 9(b) shows the comparison of the hysteresis loops. From figure 9, it is clearly observed that the model prediction results correspond well with the experimental results with a maximum error of less than 2.5% of the total range.

Table 1. Coefficients of the hysteresis model.

Numbers	r_i	b_i	a_i
1	0.01	0.5125	−0.0013
2	0.1183	0.4244	−0.0341
3	0.3349	0.0533	0
4	0.4431	0.0639	0.2819
5	0.5514	0.0424	
6	0.6597	0.0288	
7	0.7680	0.0707	
8	0.8763	0.0718	
9	0.9846	0.0230	
10	1.2011	0.1411	
11	1.4177	0.0193	
12	1.5260	0.0163	
13	1.8508	0.1681	
14	2.0674	0.1685	

3.3. Experimental verification

In this section, a series of excitation signals with different amplitudes and frequencies are utilized to validate the modeling and identification approaches for the GMMA.

The experimental results are shown in figures 10–12. Figure 10 shows comparisons of the experimental output and the developed model prediction output under different amplitude currents, where the amplitude-dependent hysteresis loops of the GMMA are predicted. Figure 11 shows the comparisons for different frequency input signals with frequencies up to 100 Hz. From figures 10 and 11, it can be seen that the comprehensive model developed can predict the hysteresis behaviors of the GMMA well. In order to further address the validity of the proposed comprehensive model, figure 12 shows the prediction performance and modeling error under a complex harmonic excitation. Therefore, we can demonstrate that the proposed model and the identified parameters account well for both the dynamic characteristics and hysteresis nonlinearity of the tested GMMA. It should be noted that we focus on a comprehensive modeling approach for the GMMA based on complete descriptions of nonlinear electro-magnetic behavior, the magnetostrictive effect and the frequency response of the mechanical dynamics. The

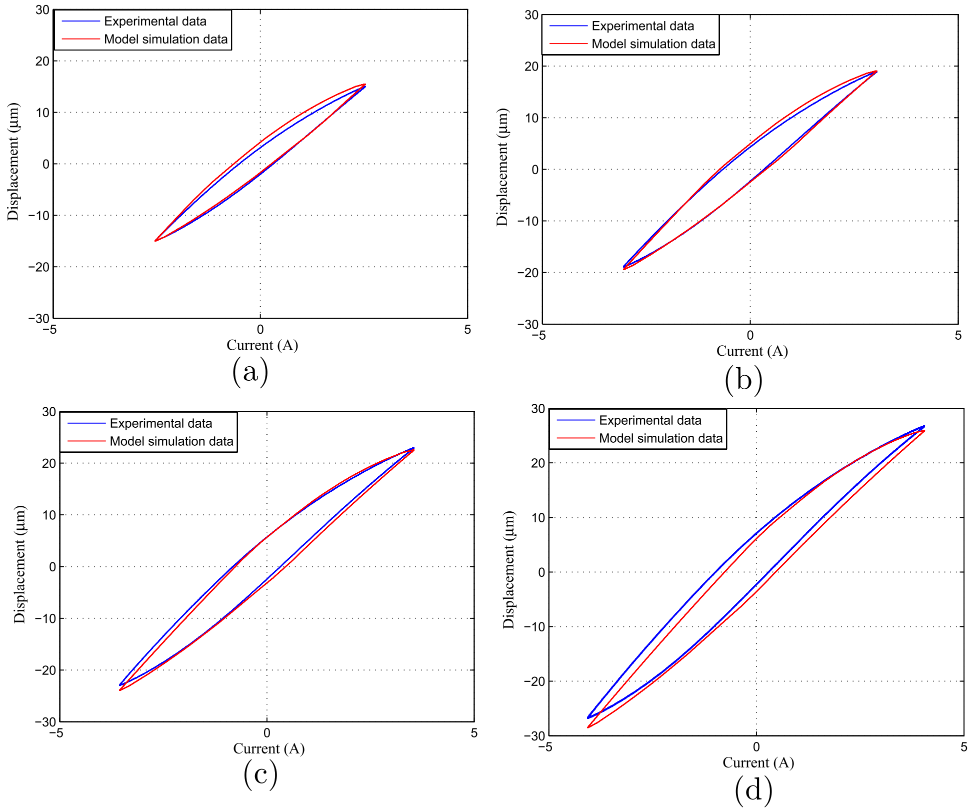

Figure 10. Model validation with different amplitude input signals. (a) Driving current: $2.5\sin(2\pi t)$. (b) Driving current: $3.0\sin(2\pi t)$. (c) Driving current: $3.5\sin(2\pi t)$. (d) Driving current: $4.0\sin(2\pi t)$.

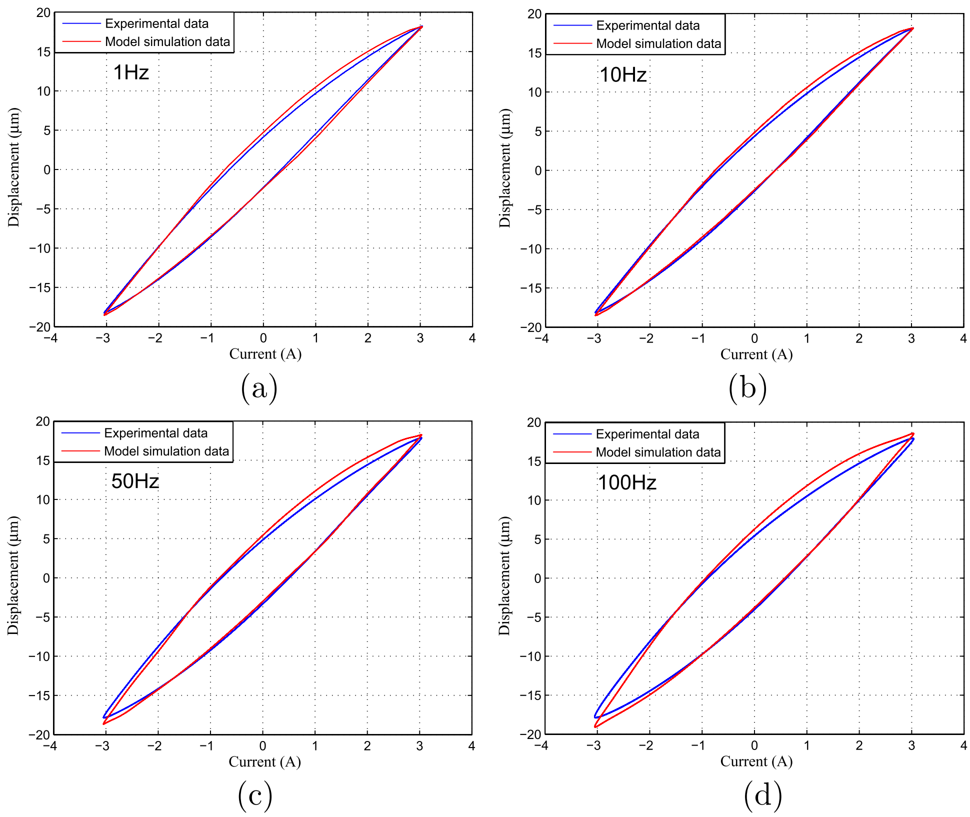

Figure 11. Model validation with different frequency input signals. (a) Driving current: $3.0\sin(2\pi t)$. (b) Driving current: $3.0\sin(2\pi \times 10t)$. (c) Driving current: $3.0\sin(2\pi \times 50t)$. (d) Driving current: $3.0\sin(2\pi \times 100t)$.

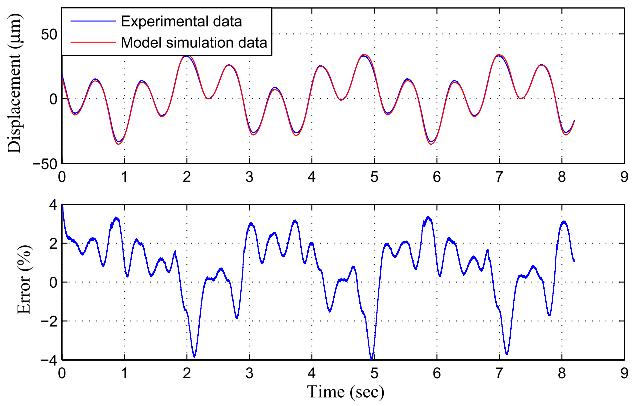

Figure 12. A complex harmonic excitation: $i(t) = 4\sin(8.80t) + 2.5\sin(2.51t + \pi/2)$.

rate-independent hysteresis model (12) is employed to validate the proposed modeling approach. In the experiments, the maximum frequency for the validation is 100 Hz, as shown in figure 11. In order to validate the proposed model with even higher frequencies, the rate-dependent hysteresis model should be used. In this work, the model development for rate-dependent hysteresis behavior is not considered because there is no a general model for the rate-dependent hysteresis description of the GMMA. In fact, modeling the rate-dependent hysteresis itself is an interesting and challenging research topic [41–43]. It will be investigated in the future on the basis of this work.

4. Conclusion

In this paper, a novel comprehensive modeling approach for GMMAs is proposed and a corresponding identification method is presented. To verify the effectiveness of the proposed model and the identification method, a prototype platform is established and experimental tests with a series of excitation signals are conducted. The experimental results clearly demonstrate the excellent performance of the proposed modeling approach. Several distinct features of this paper are summarized as follows.

(i) A comprehensive dynamic model of the GMMA is developed based on descriptions of nonlinear electromagnetic behavior, the magnetostrictive effect and the frequency response of the mechanical dynamics. It maps the relationships between current and magnetic flux at the electromagnetic part to force and displacement at the mechanical part in a lumped parameter form. Thus, the proposed model can be characterized as a linear dynamic plant proceeded by an input hysteresis nonlinearity.

(ii) To identify the comprehensive model, the linear dynamic part and the nonlinear hysteresis part are estimated separately. For the linear part, an ADT based approach is used based on both the transient-response and frequency-response data. Then, a MPI model is introduced to describe the hysteresis nonlinearity and a constrained quadratic optimization method is adopted to identify its parameters.

(iii) An experimental platform with the GMMA is established. Experimental tests with a series of excitation signals are conducted to verify the effectiveness of the proposed comprehensive model and the corresponding identification method.

Acknowledgments

This work was supported by China Postdoctoral Science Foundation under Grant 2013M530193, and the National Natural Science Foundation of China under Grant Nos 91023047 and U1201244.

References

[1] Devasia S, Eleftheriou E and Moheimani S O R 2007 A survey of control issues in nanopositioning *IEEE Trans. Control Syst. Technol.* **15** 802–23
[2] Gu G Y, Zhu L M, Su C Y and Ding H 2013 Motion control of piezoelectric positioning stages: modeling, controller design and experimental evaluation *IEEE/ASME Trans. Mechatronics* **18** 1459–71
[3] Valadkhan S, Morris K and Khajepour A 2009 Review and comparison of hysteresis models for magnetostrictive materials *J. Intell. Mater. Syst. Struct.* **20** 131–42
[4] Valadkhan S, Morris K and Shum A 2010 A new load-dependent hysteresis model for magnetostrictive materials *Smart Mater. Struct.* **19** 125003
[5] Liu H, Jia Z, Wang F and Zong F 2012 Research on the constant output force control system for giant magnetostrictive actuator disturbed by external force *Mechatronics* **22** 911–22
[6] Claeyssen F, Lhermet N, Letty R L and Bouchilloux P 1997 Actuators, transducers and motors based on giant magnetostrictive materials *J. Alloys Compounds* **258** 61–73
[7] Olabi A G and Grunwald A 2008 Design and application of magnetostrictive materials *Mater. Des.* **29** 469–83
[8] Davino D, Giustiniani A and Visone C 2011 A two-port nonlinear model for magnetoelastic energy-harvesting devices *IEEE Trans. Ind. Electron.* **58** 2556–64
[9] Su C Y, Wang Q Q, Chen X K and Rakheja S 2005 Adaptive variable structure control of a class of nonlinear systems with unknown Prandtl–Ishlinskii hysteresis *IEEE Trans. Autom. Control* **50** 2069–74
[10] Jiles D C and Atherton D L 1986 Theory of ferromagnetic hysteresis *J. Magn. Magn. Mater.* **61** 48–60
[11] Jiles D C and Li L 2004 A new approach to modeling the magnetomechanical effect *J. Appl. Phys.* **95** 7058–60
[12] Smith R C, Dapino M J, Braun T R and Mortensen A P 2006 A homogenized energy framework for ferromagnetic hysteresis *IEEE Trans. Magn.* **42** 1747–69
[13] Rosenbaum S, Ruderman M, Strohla T and Bertram T 2010 Use of Jiles-Atherton and Preisach hysteresis models for inverse feed-forward control *IEEE Trans. Magn.* **46** 3984–9
[14] Bertotti G and Mayergoyz I D 2006 *The Science of Hysteresis: Mathematical Modeling and Applications* (New York: Academic)
[15] Tan X and Baras J S 2004 Modeling and control of hysteresis in magnetostrictive actuators *Automatica* **40** 1469–80
[16] Davino D, Natale C, Pirozzi S and Visone C 2004 Phenomenological dynamic model of a magnetostrictive actuator *Physica* B **343** 112–6

[17] Ruderman M and Bertram T 2010 Discrete dynamic Preisach model for robust inverse control of hysteresis systems *49th IEEE Conf. on Decision and Control* pp 3463–8
[18] Ma Y, Mao J and Zhang Z 2011 On generalized dynamic Preisach operator with application to hysteresis nonlinear systems *IEEE Trans. Control Syst. Technol.* **19** 1527–33
[19] Machi J W, Nistri P and Zecca P 1993 Mathematical models for hysteresis *SIAM Rev.* **35** 94–123
[20] Kuhnen K and Krejci P 2009 Compensation of complex hysteresis and creep effects in piezoelectrically actuated systems—a new Preisach modeling approach *IEEE Trans. Autom. Control* **54** 537–50
[21] Gu G Y, Yang M J and Zhu L M 2012 Real-time inverse hysteresis compensation of piezoelectric actuators with a modified Prandtl–Ishlinskii model *Rev. Sci. Instrum.* **83** 065106
[22] Dapino M J, Smith R C and Flatau A B 2000 Structural magnetic strain model for magnetostrictive transducers *IEEE Trans. Magn.* **36** 545–56
[23] Armstrong W D 2002 A directional magnetization potential based model of magnetoelastic hysteresis *J. Appl. Phys.* **91** 2201–10
[24] Bottauscio O, Chiampi M, Lovisolo A, Roccato P E and Zucca M 2008 Dynamic modeling and experimental analysis of Terfenol-D rods for magnetostrictive actuators *J. Appl. Phys.* **103** 07F121
[25] Braghin F, Cinquemani S and Resta F 2011 A model of magnetostrictive actuators for active vibration control *Sensors Actuators* A **165** 342–50
[26] Grunwald A and Olabi A G 2008 Design of a magnetostrictive (MS) actuator *Sensors Actuators* A **144** 161–75
[27] Oates W S, Evans P G, Smith R C and Dapino M J 2009 Experimental implementation of a hybrid nonlinear control design for magnetostrictive actuators *J. Dyn. Syst. Meas. Control* **131** 041004
[28] Sablik M J and Jiles D C 1993 Coupled magnetoelastic theory of magnetic and magnetostrictive hysteresis *IEEE Trans. Magn.* **29** 2113–23
[29] Kuhnen K, Schommer M and Janocha H 2007 Integral feedback control of a self-sensing magnetostrictive actuator *Smart Mater. Struct.* **16** 1098–108
[30] Engdahl G and Bergqvist A 1996 Loss simulations in magnetostrictive actuators *J. Appl. Phys.* **79** 4689–91
[31] Jin K, Kou Y, Liang Y and Zheng X 2011 Effects of hysteresis losses on dynamic behavior of magnetostrictive actuators *J. Appl. Phys.* **110** 093908
[32] Tan X B and Iyer R V 2009 Modeling and control of hysteresis *IEEE Control Syst. Mag.* **15** 26–9
[33] Gu G Y, Zhu L M and Su C Y 2014 Modeling and compensation of asymmetric hysteresis nonlinearity for piezoceramic actuators with a modified Prandtl–Ishlinskii model *IEEE Trans. Ind. Electron.* **61** 1583–95
[34] Ackerman A E, Liang C and Rogers C A 1996 Dynamic transduction characterization of magnetostrictive actuators *Smart Mater. Struct.* **5** 115–20
[35] Engdahl G 2000 *Handbook of Giant Magnetostrictive Materials* (New York: Academic)
[36] Goldfarb M and Celanovic N 1997 Modeling piezoelectric stack actuators for control of micromanipulation *IEEE Control Syst. Mag.* **17** 69–79
[37] Zhang Z, Mao J and Zhou K 2013 Experimental characterization and modeling of stress-dependent hysteresis of a giant magnetostrictive actuator *Sci. China Technol. Sci.* **56** 656–65
[38] Janaideh M A, Rakheja S and Su C Y 2009 A generalized Prandtl–Ishlinskii model for characterizing the hysteresis and saturation nonlinearities of smart actuators *Smart Mater. Struct.* **18** 045001
[39] Giri F, Rochdi Y, Chaoui F Z and Brouri A 2008 Identification of Hammerstein systems in presence of hysteresis-backlash and hysteresis-relay nonlinearities *Automatica* **44** 767–75
[40] Li J W, Chen X B and Zhang W J 2011 Axiomatic-design-theory-based approach to modeling linear high order system dynamics *IEEE/ASME Trans. Mechatronics* **16** 341–50
[41] Davino D, Natale C, Pirozzi S and Visone C 2004 Rate-dependent losses modeling for magnetostrictive actuators *J. Magn. Magn. Mater.* **272** 1781–2
[42] Hovorka O, Evans R, Friedman G and Chantrell R 2012 Rate-dependent hysteresis losses in ensembles of magnetic nanoparticle clusters *Bull. Am. Phys. Soc.* **57** Q13.008
[43] Hu Z, Smith R C and Ernstberger J M 2012 Data-driven techniques to estimate parameters in a rate-dependent ferromagnetic hysteresis model *Physica* B **407** 1394–8